

Two-dimensional fluid viscosity measurement in microchannel flow using fluorescence polarization imaging

Reiko KURIYAMA^{†*}, Tomotaka NAKAGAWA[†], Kazuya TATSUMI[†], Kazuyoshi NAKABE[†]

5

[†] Department of Mechanical Engineering and Science
Graduate School of Engineering, Kyoto University
Kyoto daigaku-katsura, Nishikyo-ku, Kyoto 615-8540, JAPAN
Tel: +81-75-383-3608 Fax: +81-75-383-3608

10

* To whom correspondence should be addressed.
E-mail: kuriyama.reiko.2m@kyoto-u.ac.jp

Abstract

15 This study describes the development of a non-contact and two-dimensional fluid viscosity measurement technique which is based on fluorescence polarization microscopy. This technique exploits fluorescence depolarization due to rotational Brownian motion of fluorophores and determines fluid viscosity in microchannel flow by measuring steady-state fluorescence polarization. The main advantage of the technique is that planar distributions of fluid viscosity can be visualized by non-contact optical measurement, while commonly used mechanical viscometers measure viscosity of bulk liquids. Moreover, steady-state polarization measurements are realized by a simple experimental setup compared to other non-contact techniques such as time-resolved fluorescence lifetime/polarization measurements. The relationship between the fluid viscosity (μ) and the fluorescence polarization degree (P) was experimentally obtained by using casein molecules labeled with fluorescein isothiocyanate as a fluorescent probe. The fluid viscosity was controlled within the range of 0.7–3.0 mPa·s, which is often encountered in the biological materials, by mixing sucrose or glucose with the solution. The fluid temperature was maintained uniform at 30 °C during the measurement. The calibration result showed that $1/P$ linearly increased with $1/\mu$ which agreed qualitatively well with the theoretical prediction. The measurement uncertainty was 7.5–9.5% based on the slope of the calibration curve. Viscosity gradient generated by the mass diffusion between the two solutions co-flowing in the Y-shaped microchannel was clearly visualized under uniform temperature condition by applying the calibration curve. Finally, the influence of the temperature change on P was experimentally evaluated. The results supported the applicability of the present technique for visualization of the viscosity distribution induced by temperature change. These results confirmed the feasibility of the present technique for analyzing microscale viscosity fields associated with mass transport or temperature change.

20
25
30
35

Keywords

Fluid viscosity, Microchannel flow, Fluorescence polarization, Rotational Brownian motion, Two-dimensional distribution, Polarization degree

5 1. Introduction

In recent years, the drastic advances in microfabrication techniques have stimulated the miniaturization and integration of chemical and biochemical analysis systems. Such integrated systems, termed micro total analysis systems and lab-on-a-chip devices [1-3], offer several advantages; reducing the size of the device, reduction of sample and waste volume, high throughput in multiplexed processing, shorter analysis time, and low unit cost. For designing and developing these systems, it is essential to understand flow behavior and mass transport in microchannel, where various operations including sample injection, concentration, mixing, reaction, separation, and detection take place. Fluid viscosity depends on solute concentration and temperature, and can change over space and time in microchannel during the above operations. This leads to the changes in flow field, diffusion coefficient and the species distributions[4,5], which eventually affects fluid viscosity in a coupled manner. Thus, determination of local viscosity in microscopic scale is an important issue in terms of detailed understanding of the flow structure, mass transport and hydrodynamic effect. It also provides useful and quantitative information for evaluating chemical processes and mixing performance in the microfluidic systems, since fluid viscosity is linked with composition change and transport of chemical components in the sample solution. In addition to this, microscale viscosity mapping is useful for analyzing biological samples such as cells and blood plasma for biomedical applications.

A variety of methods for measuring fluid viscosity have been developed to date. Conventional mechanical viscometers, such as tube viscometers and rotational viscometers [6] have been widely used in various researches and industries. These methods determine the viscosity of bulk liquids, i.e., viscosity averaged over the whole sample, using the relationship between strain rate and shear stress. Over the last decade, many researchers have addressed the miniaturization of viscometers to reduce sample volume and proposed different kinds of microfluidic viscometers[7-12]. These devices are based on various operating principles, such as microfluidic capillary viscometers[7], microchannels equipped with pressure sensors[8], microcantilevers[9], microchannels employing laminar parallel flows[10,11] and droplet-based viscometer with flow-focusing geometry[12]. They, however, focus on characterization of rheological properties of bulk sample inside the specifically-designed channels or flow cell rather than in-situ measurement of local viscosity in generic microfluidic devices.

To achieve in-situ and local measurements of fluid viscosity in microscopic scale, optical-based techniques are promising. One approach is to use synthetic fluorescent probe whose fluorescence emission is sensitive to the viscosity of the surrounding environment.

Molecular rotors[13,14] are representative viscosity probes, in which fluorescence intensity and lifetime are altered depending on intramolecular torsional or rotational dynamics in excited state. They have been used for mapping heterogeneous viscosity distribution especially in a biological environment including live cells. In such imaging applications, fluorescence lifetime imaging [15], ratiometric fluorescence imaging [16], and polarization technique [17] can provide higher accuracy compared to intensity-based measurement since intensity-based method is difficult to be coupled with the viscosity variation due to the spatial variation of probe concentration and excitation intensity. More recently, fluorophores with different structural design have also been proposed as a viscosity probe, in which emission wavelength changes with flapping-like conformational change of the fluorophore[18].

Another optical approach is to exploit translational or rotational Brownian motion of small particles and fluorophores. Dynamic light scattering[19], Brownian microscopy[20], fluorescence recovery after photobleaching[21], and fluorescence correlation spectroscopy[22] are the methods in which one monitors translational diffusion kinetics of Brownian particles and determines viscosity of the surrounding medium based on Stokes–Einstein equation. There are also the methods for probing rotational diffusion of fluorophores, such as time-resolved and steady-state fluorescence polarization methods. Both methods exploit fluorescence depolarization due to the rotational Brownian motion of fluorophores, but the former analyzes the dynamics of the fluorescence emission [23,24] while the latter observes the fluorescence integrated over the fluorescence lifetime[24-26].

Among these techniques, the present study employs steady-state fluorescence polarization (also known as fluorescence anisotropy). When fluorophores dissolved in fluid are exposed to a linearly-polarized light, they experience rotational Brownian motion during the fluorescence lifetime, and as a consequent, the polarization direction of the fluorescence shows greater randomness. This results in a decrease in polarization degree of the fluorescence, i.e., fluorescence depolarization. The degree of the depolarization is mainly determined by the extent of the Brownian rotation, which is related to the fluid temperature, viscosity, and the molecular size. Therefore, these parameters can be probed by polarization measurement. Based on this physics, this method has long been a popular tool mainly for analyzing interactions and binding of biomolecules in clinical and biochemical assays[27,28]. Furthermore, fluorescence polarization method can easily be applied to microscopic measurement in combination with optical microscope and thus has already been used for microfluidic applications. Some groups have developed microchip-based analysis systems for various biological reactions such as immunoassays and protein-protein binding [29-31]. The authors' group has evaluated the relationship between the fluorescence polarization degree and the fluid temperature, and performed measurements of two-dimensional temperature distribution in a microchannel [32,33].

In the present study, we focus on a development of a technique for in-situ and two-dimensional viscosity mapping in microchannel flow based on steady-state fluorescence polarization. The main advantage of employing this technique for viscosity measurement is

that two-dimensional distributions can be visualized at micron resolution with relatively simple experimental setup, compared to time-resolved measurements. Moreover, unlike the techniques using molecular rotors, any fluorophore can be used as a probe, providing it possesses an adequate molecular size and fluorescence lifetime for detection of depolarization. In addition, polarization measurement is less susceptible to sample heterogeneity and environmental disturbance (such as inhomogeneity of fluorophore concentration, spatio-temporal variation in excitation intensity, and quenching effect by pH change) than fluorescence intensity measurement, which makes the technique useful especially for imaging applications. It should be stated, however, that the present technique as well as many other optical approaches measures “local viscosity” which can be sensed by nanoscale fluorophores, and it may be different from the “viscosity in bulk” measured by mechanical approaches especially in complex fluids. That is, the viscosity measured by the present technique is expected to be less influenced by the existence of particles and networks (such as blood cells and polymer entanglements) in liquids.

The rest of this paper is organized as follows. First, measurement principle is detailed in section 2, followed by a description of the experimental methods in section 3 containing optical system for polarization measurement, microchannel and prepared slide used for sample holder, properties of the fluorophores and working fluids, and procedure of image processing. In subsection 4.1, the relationship between the polarization degree and the fluid viscosity is evaluated to examine the feasibility of the technique using three fluorophores and two solutes. The fluid viscosity is varied by changing solute concentration and the fluid temperature is maintained uniform and constant. The influences of fluorescence intensity variation and the flow field on polarization measurement are discussed in subsection 4.2. We also comment on some point which should be considered when applying the present method. In subsection 4.3, we demonstrate a two-dimensional measurement for the mass diffusion between parallel flows of two solutions in a Y-shaped microchannel. The measurement result is compared with the result of numerical calculation to validate the present technique. Finally, in subsection 4.4, the influence of the temperature change on polarization degree is evaluated to examine the applicability of the present technique for measurement of the viscosity distribution associated with temperature change.

2. Measurement Principle

Figure 1 illustrates the polarization characteristics of fluorescence, which is determined by the relative angle between the polarization directions of the excitation light and the absorption/emission moments of the fluorophore. When fluorophores are irradiated by a linearly polarized excitation light, only those with the absorption moments appropriately aligned to the excitation polarization direction can absorb the light. Specifically, the probability of the absorption is proportional to the value $\cos^2 \theta$, where θ represents the angle between the directions of the excitation polarization and the absorption moment. Hence, the absorption rate is maximum when the absorption moment of the fluorophore is parallel to the polarization direction of the excitation light ($\theta = 0^\circ$) and the absorption rate decreases to 0

contrastingly when the absorption moment is perpendicular to the excitation light ($\theta = 90^\circ$).

When the fluorophores are excited (at the time $t = 0$), they emit fluorescence polarized in the direction of the emission moment during their fluorescence lifetime (at $t \sim \tau$). The directions of absorption and emission moments of the fluorophore can be assumed to be identical in general. Therefore, when an infinite number of randomly oriented fluorophores are exposed to a linearly polarized excitation light, molecules are stochastically excited and emit fluorescence with the probability depending on θ . As a result, the observed fluorescence is partially polarized with the maximum intensity component in the same direction with the excitation light. The lower part of figure 1 shows the probability density distributions of θ for absorption and emission. If the molecules are at stationary state (figure 1(a)), they emit fluorescence polarized in the same direction of the absorption moment at $t = 0$. Therefore, the probability density distributions for absorption and emission overlap each other. On the other hand, if the fluorophores are suspended in fluid (figure 1(b)), they can rotate and experience rotational Brownian motion during the period from excitation to emission. Consequently, the emission moments at $t = \tau$ are randomized depending on the extent of their rotation. This makes the probability density distribution for emission broadened and thus the observed fluorescence is depolarized compared with the case of stationary condition with the degree which is related to the fluid viscosity, temperature, the molecular size, and the fluorescence lifetime. This is the fluorescence depolarization due to the rotational Brownian motion of fluorophores.

The degree of fluorescence polarization can be evaluated by polarization degree, P , which is defined as follows:

$$P = (I_{\parallel} - I_{\perp}) / (I_{\parallel} + I_{\perp}), \quad (1)$$

where I_{\parallel} and I_{\perp} are the fluorescence intensities of the components that are parallel and perpendicular to the polarization direction of the excitation light, respectively. Perrin[34] and Weber[35] theoretically derived the equation which relates P value to the fluorescence lifetime and the rotational diffusion of fluorophores as follows:

$$\left(\frac{1}{P} - \frac{1}{3} \right) = \left(\frac{1}{P_0} - \frac{1}{3} \right) \left(1 + \frac{k_B T \tau}{\mu V} \right), \quad (2)$$

where k_B [J/K] is the Boltzmann constant, V [m³] is the hydrodynamic volume of the rotating unit, and τ [s] is the fluorescence lifetime. T [K] and μ [Pa·s] are the absolute temperature and viscosity of the fluid, respectively. P_0 is the intrinsic or limiting polarization defined as the polarization degree of the molecule at stationary condition (in the absence of rotation), and it shows constant value of 0.5 when absorption and emission moments are collinear.

Clearly seen from equation (2), the reciprocal of P has a linear relationship with T/μ . Therefore, if V and τ remain constant during the measurement, the fluid viscosity μ can be determined by measuring P under fixed temperature condition. The proposed technique measures fluid viscosity based on this principle. It should be noted that both fluid viscosity and temperature influence the P value and that their influences cannot be distinguished from each other. The present study basically focuses on the measurement of fluid viscosity under known uniform temperature. Therefore, the calibration between viscosity and the polarization degree is carried out by changing solute concentration (in subsections 4.1-4.2), and the calibration result is applied to the flow field at the same temperature condition (in subsection 4.3). The applicability of the calibration result to the viscosity field under varying temperature condition will be discussed in subsection 4.4.

Polarization-based measurement is advantageous for imaging application compared to intensity-based measurement since it is less influenced by spatial heterogeneity of the sample and external disturbances. When attenuation of excitation light and re-absorption of fluorescence emission are negligible, the fluorescence intensity observed from fluorophore solution, I_f [W m^{-2}], is expressed as the following equation [36]:

$$I_f = A I_e C \phi \varepsilon L, \quad (3)$$

where A [-] is the collection efficiency of the detection system, I_e [W m^{-2}] is the excitation intensity, C [mol l^{-1}] is the concentration of fluorophores, ϕ [-] is the quantum efficiency, ε [$\text{l mol}^{-1} \text{m}^{-1}$] is the molar absorption coefficient, and L [m] is the length along the optical path of the excitation light. Generally, excitation intensity and fluorophore concentration are not uniform over the measurement area and can temporally fluctuate during the experiment. In addition, the quantum efficiency is susceptible to pH and the quencher concentration in the sample fluid. Although these above factors significantly influence the fluorescence intensity, polarization degree P is less influenced since it is normalized by the fluorescence intensity ($I_{\parallel} + I_{\perp}$) as equation (1) and follows the rotational motion of the fluorophores only. This leads to the robust and reliable measurement of two-dimensional viscosity distribution.

3. Measurement Methods

3.1 Optical system

Figure 2 shows a schematic of the optical system for fluorescence polarization measurement, mainly consisting of an inverted microscope (Olympus; IX-73), an LED light source, polarizing elements, and two high sensitivity cameras (Andor Zyla; 4.2 PLUS, 2048×2048 pixels, 16bit). The LED light was linearly polarized by a polarizer (Edmund; #47216), filtered by a bandpass filter and was focused to the sample by an objective lens (Olympus; LMPlanFL N, 10x). The fluorescence emitted from the sample was collected by the same objective lens, filtered by another bandpass filter and split into two components (I_{\parallel}

and I_{\perp}) by a polarizing prism (Thorlabs; PBS251). I_{\parallel} and I_{\perp} were simultaneously measured by camera 1 and camera 2, respectively. The exposure time was set at 1.0 s and the camera was operated at the fastest readout rate, which corresponds to the frame rate of 0.990 for full image (2048×2048 pixels). The total magnification of the system was approximately 10.2 and the spatial resolution was calculated to be $0.64 \mu\text{m}/\text{pixel}$ using the magnification of the pixel size of the camera ($6.5 \mu\text{m}$). In the present study, only the low-magnification objective lens was used for the measurement. Therefore the obtained fluorescence images show the intensity distribution integrated over the whole sample height although the focal plane of the objective lens was set at the middle height of the microchannel. The temperature of the microscope stage was controlled by circulating water from an isothermal bath (As One; LTCi-150H) so that the fluctuation and deviation of the sample temperature was maintained within $\pm 0.5^{\circ}\text{C}$ from the set temperature. In addition, the temperature uniformity of sample on the temperature controlling stage was examined using thermocouples prior to the measurement. The thermocouples were attached to the upper surface of a cover glass on the stage along the center line with equal spacing of 1mm. The temperature variation among of the three was within $\pm 0.2^{\circ}\text{C}$. Note that the LED light source and the set of optical filters were appropriately selected with consideration of the fluorescence characteristics of the fluorophores. Table 1 shows the list of optical components for each fluorophore used in this study.

In the present study, two-camera configuration is employed for polarization measurement since it can obtain two polarizing intensities I_{\parallel} and I_{\perp} simultaneously and thus provide accurate results even if the fluorescence intensity changes over time due to the various factors such as variations of excitation intensity and fluorophore concentration, and fluorescence degradation. It is also advantageous for the measurements in unsteady flows. In one-camera configuration, on the other hand, two polarizing intensities are obtained with some time lag by rotating or switching the polarizers. However, it can be used for the measurement in steady flows if this time lag is sufficiently small compared to the time scale of the fluorescence intensity variation.

3.2 Prepared slide and microchannel

Sample solution was filled in a prepared slide or supplied to a composite microchannel at a constant flow rate using a syringe pump (Nihon Koden; CFV-3200). The prepared slide consisted of bottom and upper cover glasses spaced by two strips of $120 \mu\text{m}$ thick parafilm and was used for the experiments on probe selection. The microchannel was comprised of poly(dimethylsiloxane) (PDMS) chip and a silica glass slide. The channel structure was $30\text{--}40 \mu\text{m}$ tall, molded in a PDMS layer by soft lithography, and bonded to the cover glass by oxygen-plasma treatment. A straight PDMS microchannel (figure 3(a)) was used for calibration experiment and a Y-shaped microchannel (figure 3(b)) was used for measurement of viscosity distribution. Teflon tube was used to connect the inlet of the microchannel and a glass syringe (Hamilton; 1001LT) set on the syringe pump. The aspect ratio (the ratio of

channel height to width) of the microchannel is small enough (~ 0.07) to assume the channel flow as two-dimensional. To monitor the channel temperature during the polarization measurement, K-type thermocouples of 100 μm in diameter were attached to the cover glass of the prepared slide or inserted in 1-mm diameter holes of PDMS chip. The signal from the thermocouples was acquired by a data logger (National Instruments; NI-9219) and converted to the temperature.

3.3 Fluorophores and working fluids

The present study employed uranine (Nacalai Tesque, #3581692), rhodamine B (Nacalai Tesque, #3010822) and casein molecules labeled with fluorescein isothiocyanate (AAT Bioquest; #13440; C-FITC) as fluorescent probes. The properties of these fluorophores are summarized in table 2. The concentration of the fluorophore was set to be $1.0 \times 10^{-4} \text{ mol/l}$ for uranine and rhodamine B solutions, and $4.0 \times 10^{-5} \text{ mol/l}$ for C-FITC solution in the present study.

Aqueous solution was used as working fluid. Sucrose or glucose was added to pure water for adjusting the fluid viscosity. In anticipation of the future application to biological materials, the viscosity of sample solution in the present study was controlled in the range 0.7 –3.0 $\text{mPa}\cdot\text{s}$ at 30°C. The relationships between the solute concentration and the solution viscosity at 30°C were acquired preliminarily by viscosity measurement using a rheometer (Anton Paar; MCR301). The measured values were fitted by third-order polynomial regression function, which was used for viscosity estimation for solution of known concentration.

3.4 Image processing

In this section, the procedure for calculating the distribution of polarization degree is described in detail. The coordinates of the images detected by the two cameras were precisely registered by employing the below image processing to obtain the polarization degree on a pixel-by-pixel basis. A glass plate with a grid pattern (line width: 10 μm , spacing: 100 μm) was used as a calibration target and positioned on the microscope stage. The grid pattern image was acquired by each camera via transmission illumination using a halogen lamp and then intersections of the grid lines were extracted as reference points. The number of the grid points imaged in a whole image of 2048 \times 2048 pixels was up to 169 and the typical number of the reference points which could be extracted by image processing was ~ 150 out of 169. The coordinates of the image plane of camera 2 were registered to those of camera 1 affine transformation [44,45] using the pixel positions of the corresponding pairs of reference points. This image registration method can describe image deformations including scaling, rotation, shear, translation and reflection, although only translation, rotation and reflection between two image planes were observed in the present study. By using the obtained affine transformation matrix, the image plane of camera 2 was transformed into alignment with that of camera 1 at the accuracy of about 0.5 pixels on average, which corresponds to about 0.33 μm in physical plane. Since affine transformation cannot describe curvature or twist, a more advanced

method using non-linear terms [45,46] should be employed when the image distortion is non-negligible.

Fluorescence images, which were simultaneously acquired by two cameras in the polarization measurement, were registered to one another by using the affine transformation matrix obtained in the above procedure and converted into distributions of polarization degree using equation (2). Figure 4(a) shows a typical example of P distribution ($640 \times 320 \mu\text{m}^2$) obtained from 35wt% sucrose solution with C-FITC molecule. Although the sample is homogeneous and therefore the viscosity is uniform over the measurement area, there exists a spatial pattern in the P distribution, which results in the considerable error in viscosity measurement (approximately 7.7%). This pattern was found for all samples, and thus it could be a kind of systematic error arising from the spatial distribution of efficiency of optical components (including camera sensitivity and transmission of filters). Dusts attached to the optical components are also responsible for the spatial pattern. In the present study, influence of this fixed pattern in the polarization degree was eliminated as following: a spatial average \bar{P}_i was calculated for each of polarization degree distributions $P_i(x, y)$ which were obtained under uniform viscosity conditions. \bar{P}_i was then subtracted from the value of each position $P_i(x, y)$ to derive the distribution of deviation $B_i(x, y)$. Finally, the ensemble average $B(x, y)$ was calculated and subtracted from each of the distributions $P_i(x, y)$. Figure 4(b) shows the result of the above procedure applied to the distribution in figure 4(a) and presents a uniform distribution over the measurement area. The standard deviation of P values in the distribution was reduced from 1.43% to 0.42%, which corresponds to the error of 2.1% in viscosity measurement.

4. Results and Discussion

4.1 Selection of fluorescent probe

As one can see in equation (2), P theoretically decreases with $1/\mu$ under an isothermal fluid condition and the slope changes with τ and V . Therefore, the sensitivity and precision of the viscosity measurement highly depend on the characteristic properties of the fluorescent probe. To select a suitable probe for the present viscosity range (0.7–3.0 mPa·s), polarization measurement was carried out using uranine, rhodamine B and C-FITC which were added to sucrose solution. Sample solutions were filled in a prepared slide or microchannel and remained at rest in both cases (i.e., no flow condition). 10 pairs of fluorescence images were obtained for each condition.

Figure 5 shows the relationship between the measured polarization degree P and the reciprocal of fluid viscosity μ . Each plot shows the time and spatial averaged value. The theoretical values for the fluorophores derived by equation (2) are also shown in solid lines for reference. The properties of fluorophores (in table 2) were applied for the calculation and the hydrodynamic volume V was calculated by assuming the fluorophore as a rigid sphere with the given diameter. In figure 5, the measured P values decreased with $1/\mu$ in all cases, which is reasonable since the degree of the Brownian motion gets intense with decreasing

viscosity and thus the direction of the emission moments are randomized. In uranine and rhodamine B cases, the viscosity dependence of P obtained by polarization measurement shows qualitatively similar trend with the theoretical result, although there are some difference in the absolute values. On comparison of these two molecules, rhodamine B shows larger P values, which is due to its larger molecular volume and shorter fluorescence lifetime compared to uranine.

In the C-FITC case, on the other hand, experimental and theoretical values are substantially different. The experimental result shows the averaged value of four measurements and the error bars show the 95% confidence interval (considering the variations in polarization measurement and viscosity measurement). The experimental result shows a considerable decrease in P with increasing $1/\mu$, similar to those of uranine and rhodamine B cases, while theoretical prediction shows almost constant P value at 0.5. This difference between theory and experiment is attributed to the molecular structure of C-FITC. C-FITC is a casein molecule whose surface is labeled with several FITCs. Since the molecular weight (Mw) of FITC is ~ 389 , the number of FITCs linked to a single casein molecule is estimated to be ~ 20 based on the difference in molecular weight between κ -casein (Mw ~ 19000) and C-FITC (Mw ~ 26000). In calculating the theoretical value in figure 5, we assumed that the FITC molecules are fixed to the surface of the casein molecule and cannot rotate relative to the casein. Therefore, only the depolarization due to the rotation of casein molecule was taken into account in the calculation. Since the diameter of the casein is large (~ 30 nm), P remained constant near 0.5 and was not affected by the fluid viscosity. However, the experimental result infers that the FITC molecules are able to rotate on casein molecule to some degree and therefore the polarization degree exhibits viscosity dependence in reality.

Moreover, the measured P values for C-FITC are noticeably small compared to the theoretical prediction, which is attributed to the phenomenon called concentration depolarization [42]. When the separation distance between the fluorophores is sufficiently small (up to ~ 10 nm), radiationless excitation energy transfer occurs from primarily excited molecules (donors) to the surrounding unexcited molecules (acceptors). In this case, the acceptors emit depolarized fluorescence and the polarization degree of the measured fluorescence is decreased as a whole. As already mentioned, several FITCs are linked to the casein surface in a C-FITC molecule. The distances between these FITCs are considered to be small enough to incur concentration depolarization. In addition to this, concentration depolarization between neighboring C-FITCs can occur to some degree depending on the fluorophore concentration. According to the relationship between the C-FITC concentration C and the degree of concentration depolarization estimated by the theoretical equation [43] (see Supplementary Material for detail), the depolarization between neighboring C-FITCs occurs at $C > 10^{-7}$ mol/l and the fluorescence is almost completely depolarized at $C = 10^{-4}$ mol/l. From this result, C should be lower than 10^{-6} mol/l to avoid significant influence of concentration depolarization. On the other hand, such low concentration leads to the

difficulty in the measurement of weak fluorescence. To obtain sufficient intensity while suppressing the depolarization, the concentration of C-FITC was set to be 4.0×10^{-5} mol/l in the present study. The actual concentration of C-FITC solutions used in the present experiments was in the range 3.8×10^{-5} – 4.1×10^{-5} mol/l. The influence of this concentration variation within $\pm 5\%$ on measured P value is estimated to be $\pm 7 \times 10^{-4}$ based on the sensitivity of P on fluorophore concentration dP/dC , which corresponds to the viscosity value of $\pm 1.6\%$ in the present viscosity range (see Supplementary Material for detail).

Focusing on the slopes of the measured P values, they are almost comparable for the three fluorophores, and thus the sensitivities to viscosity change are considered to be equivalent in uranine, rhodamine B and C-FITC. On the other hand, the absolute value of P is the largest in the C-FITC case among the three. For example, the measured P value of C-FITC is about 0.15 at $1/\mu = 1010$ (Pa·s)⁻¹, which is 1.3 times larger than that of rhodamine B, and 2.1 times larger than that of uranine. If the fluorescence intensities of the fluorophores are in the comparable level, the difference in two polarizing intensities ($I_{||} - I_{\perp}$) becomes larger when the polarization degree P has a higher value. For example, the difference ($I_{||} - I_{\perp}$) is doubled if P value increases two-fold, which makes the measurement less susceptible to the noise component assuming that the magnitude of noise is constant. Therefore, the signal to noise ratio and measurement reliability can be increased by using C-FITC showing the highest P value among the three. According to the above discussion, C-FITC was selected as a probe in the present study.

4.2 Calibration experiments

Prior to a two-dimensional viscosity measurement, calibration experiments were conducted using C-FITC as a probe under uniform and constant fluid temperature at 30°C. The relationship between $1/P$ and $1/\mu$ was evaluated in the calibration since a simple linear correlation was expected between these values according to equation (2). Sucrose solutions with seven different concentrations (0–35wt%) and glucose solutions with five different concentrations (0–35wt%) were used for the experiments. Each solution was supplied to the straight microchannel (figure 3(a)) by the syringe pump at constant flow rate of 0.56 μl/min during the polarization measurement. This flow rate corresponds to the cross-sectional average velocity of 0.53 mm/s and Reynolds number of 0.01–0.04. 10 pairs of fluorescence images were obtained for each sample solution, and time and spatial averaged values of P of the measurement area (1000×500 pixels which corresponds to 640×320 μm²) were calculated. The measurement area was positioned at the center of the straight microchannel with a sufficient distance from the channel inlet, where the thermal boundary layer was fully developed and fluid temperature was assumed to be uniform.

Figure 6 shows the calibration result for sucrose and glucose solutions. For the sucrose case, the results shown in figure 5 are also plotted. Each plot of sucrose solution represents the averaged value of four measurements and the error bars show the 95% confidence interval (considering the variations in polarization measurement and viscosity measurement).

Similarly, plots and error bars for the glucose case were calculated from the results of three measurements. No significant difference was found between sucrose and glucose solutions with respect to the relationship between $1/P$ and $1/\mu$, which supports the versatility of the present method for viscosity measurement. $1/P$ increased linearly with $1/\mu$ as theoretically predicted by equation (2). This trend seems reasonable since molecular volume and fluorescent lifetime are assumed to be sufficiently constant in the present experiment conducted under constant temperature of $30^\circ\text{C} \pm 0.5^\circ\text{C}$. The straight lines in figure 6 were derived by least squares regression and the line obtained for sucrose solutions was used as a calibration line for the viscosity distribution measurement in the following section. The measurement uncertainty was estimated to be $0.07 \text{ mPa}\cdot\text{s}$ for $0\text{wt}\%$ sucrose solution (i.e., water) and $0.22 \text{ mPa}\cdot\text{s}$ for $35\text{wt}\%$ sucrose solution which corresponds to the measurement error of 9.5% and 7.5% , respectively.

Figure 7 shows the fluorescence intensities I and polarization degrees P of $35\text{wt}\%$ sucrose solution measured on different eight days, which are normalized by the values of Day 1. Each plot shows the time and spatial averaged value and the error bar shows the standard deviation of the spatial distribution. Although the fluorescent intensity varied significantly (more than 40%) mainly due to the differences in excitation intensity and channel height, but the polarization degree showed almost constant value (within 5%). This result enables the calibration line obtained on one certain day to be applied to a polarization distribution obtained on the other days. In addition to this, we can see that the spatial variation of P (before subtracting the systematic error B) was significantly small compared to that of I , which supports the robustness of the polarization measurement against the variation of the fluorescence intensity over space and time.

In order to examine the influence of shear flow on the rotational motion of fluorophores (FITC), the rotational angle is roughly estimated as mentioned below. Given that the velocity gradient is linear in the straight microchannel, spanwise and depthwise velocity gradients ($\delta u/\delta y$ and $\delta u/\delta z$) are calculated to be 4.0 s^{-1} and 57.1 s^{-1} , respectively, for the typical maximum flow velocity $u = 1 \text{ mm/s}$. This results in the angular velocity $\omega = 0.5((-\delta u/\delta y)^2 + (\delta u/\delta z)^2)^{1/2}$ can be estimated to be 28.6 s^{-1} and the rotational angle of $6.5 \times 10^{-6}^\circ$ during the fluorescence lifetime ($\tau \sim 4 \text{ ns}$). On the other hand, rotational angle of FITC molecule due to the rotational Brownian motion is estimated to be 55° during its lifetime (see for example section 1.2 of reference [35] for the calculation). Therefore, the influence of shear flow is negligibly small compared to Brownian rotation in typical low Reynolds number flow in microchannels. In fact, the polarization degree in the present calibration experiment showed identical value irrespective of whether sample solution was at rest or flowing (results are not shown here).

At the end of this section, we shall discuss about the applicability of this technique to measure the viscosity of complex fluids composed of large size molecules. In the present set of experiments, only solutes with low molecular weight were used for viscosity adjustment and the solute concentration was not exceedingly high. Therefore, the resultant solutions were purely Newtonian. In

this case, the viscosity of bulk sample measured by rheometer can be successfully correlated to the polarization degree P in accordance with the theoretical prediction (equation (2)). However, in the case of more complex fluids such as polymer and micellar solutions and biological fluids, the viscosity change is mainly attributed to the aggregation and formation of a network structure of the macromolecules, the scale of which is from sub-micrometer to micrometer. As a result, the bulk rheological properties are no longer correlated with the local viscosity in nanometer scale nor P values [47,48]. Although not shown here, we applied the present method to the polymer solutions containing hydroxyethyl cellulose (Daicel; SE600) and carboxymethyl cellulose (Nippon paper; F800HC), and the measured P values were much smaller than those estimated from the viscosities of the bulk fluid. In fact, the values were similar to (but slightly larger than) the values estimated from solvent viscosity. The present technique therefore cannot be used to estimate the viscosity of bulk complex fluids although it could provide some information on the microscopic environment arounds fluorophores which may interact with the macromolecules in the fluids.

4.3 Visualization of viscosity distribution in microchannel flow

Two-dimensional viscosity distribution measurement of a diffusion layer between parallel flows of two miscible solutions formed in a Y-shaped microchannel (figure 3(b)) was performed under uniform and constant temperature condition of 30°C. The 35wt% and 0% sucrose solutions with viscosity of 2.95 mPa·s and 0.78 mPa·s were supplied to each inlet at the same flow rate of 0.6μl/min by syringe pumps. Cross-sectional average velocity was 0.6 mm/s in the branched channels, and Reynolds number was calculated to be 0.01 and 0.05 for 35wt % and 0 wt% solutions, respectively. The measurement was conducted in the region shown in figure 3(c) and the two-dimensional distribution of fluid viscosity was visualized at a spatial resolution of 1.3 μm × 1.3 μm based on 2×2 pixels binning. The calibration result in figure 6 was used to convert the polarization degree to the fluid viscosity.

To examine the validity of the present technique, three-dimensional numerical computation was conducted for the viscosity distribution in the mixing layer and compared with the measurement result. A commercial finite element method computation software (COMSOL Multiphysics 4.3a) was used for the calculation. Continuity, momentum conservation equations of the flow, and binary diffusion equation were solved under steady-state laminar condition. Figure 3(d) shows the three-dimensional computational domain. The height and width were set to be same as the Y-shape microchannel used in the experiment. The computational domain was meshed with 264,810 cuboid control volumes of 7μm (x) × 5μm (y) × 2.5μm (z). No-slip condition and zero flux condition were applied to the channel walls as the boundary conditions for flow and mass concentration, respectively. Neumann condition was applied to the channel outlet. 0wt% and 35wt% sucrose-water solution were supplied from each inlet of the channel with uniform velocity distribution. In order to calculate the viscosity distribution with taking account of the concentration dependencies of transport coefficients, the concentration-dependent viscosity, density[49], and diffusion coefficient of the sucrose solution were applied to the computation. The relationship between sucrose concentration and viscosity was obtained by the measurement using the rheometer. The mutual diffusion coefficient of sucrose and

water for 30°C was obtained by linear interpolation between the literature values for 25°C and 50°C [50].

It should be noted that during the measurement, the position of the solution interface was fluctuated over time due to the pulsating flow caused by the syringe pumps. To reflect this effect on the viscosity distributions in the calculation, the positions of the solution interface of five instantaneous viscosity distributions during a period were obtained from the experiment, and the instantaneous flow rates of the solutions at each moment were evaluated. Instantaneous viscosity distributions were calculated for these flow rates and the time averaged value will be discussed here.

Figure 8(a) shows the measurement result of the time average viscosity distribution. The measured viscosities in the areas $y < 50 \mu\text{m}$ and $y > 150 \mu\text{m}$ agreed with the viscosities of 0wt% and 35wt% sucrose solutions, respectively. Further, the viscosity gradually changed in the spanwise direction in the area $50 \mu\text{m} < y < 150 \mu\text{m}$ where two fluids were in contact and diffusion takes place. We can also see that the width of the diffusion layer increases in the downstream. The diffusion layer is slightly distorted near $x = 270 \mu\text{m}$ in the measurement, which was due to the flow perturbation produced by an air bubble attached to the channel side wall. Figure 8(b) shows the viscosity distribution at the middle height of the channel obtained by the computation. The distributions of the calculation and measurement show a good agreement over the measurement area. These results show that the viscosity distribution influenced by the mass diffusion is successfully visualized by the present polarization technique.

Figure 9 shows the comparison of the spanwise distributions of the measured and calculated viscosities at the streamwise distances, $x = 10 \mu\text{m}$ and $900 \mu\text{m}$. The measured distributions agreed markedly well with the numerical calculation, quantitatively. The difference between the measured and calculated distributions in the viscosity gradients was less than 1.0%. Some deviation is observed in the area of 35wt% sucrose solution ($200 \mu\text{m} < y < 450 \mu\text{m}$), which can be accounted for by the relationship between polarization degree P and viscosity μ . The magnitude of the random error in P measurement was on the same order for the present viscosity range as shown in figure 5. However, when the error was converted to μ using the calibration result, the error in viscosity was larger in 35wt% solution than 0wt% solution. The reason for this is that the viscosity dependence of P is lower in higher viscosity range (see Supplementary Material for detail). The slope between P and μ around $0.78 \text{ mPa}\cdot\text{s}$ (0wt% sucrose solution) was approximately five times larger than that around $2.95 \text{ mPa}\cdot\text{s}$ (35wt% sucrose solution) according to the measurement result. This led to the larger deviation in the 35wt% sucrose solution area in figure 9. These results confirmed the validity of the present technique for two-dimensional measurement of viscosity distribution associated with mass transport under uniform and constant temperature condition in microchannel flow.

4.4 Evaluation of temperature effect on polarization degree

In the chapters so far, the fluid temperature was maintained uniform and constant, and the solute concentration was the cause of viscosity change. The viscosity can vary in the application due to the temperature change. For example, the temperature inside the microfluidics is often non-uniform and

changes with time due to Joule heating and chemical reactions. Therefore, we will extend the discussion a little further if the present technique can be applied to visualize the fluid viscosity change induced by the temperature variation. As seen from equation (2), the influence of the temperature change on the polarization degree P appears in two aspects: (1) direct influence due to the change in temperature T and (2) the indirect influence associated with the temperature dependence of the fluid viscosity μ . To evaluate the degree of these influences, polarization measurement was carried out at different temperature and compared with the viscosity calibration result in section 4.2. C-FITC molecule was dissolved in pure water at the concentration of 4.0×10^{-5} mol/l as the probe. The sample solution was supplied to a straight microchannel placed on a temperature-controlled stage at a constant flow rate of 3.2 μ l/min. The height and width of the microchannel was 44 μ m and 3 mm, respectively. The stage is equipped with four Peltier modules and can produce uniform temperature distribution in the channel (details are in reference [32]). The fluid temperature was changed in the range 22–40°C and monitored by two K-type thermocouples inserted in the PDMS chip. 30 pairs of fluorescence images were obtained for each temperature condition, and time and spatial averaged P values were calculated.

Figure 10(a) shows the measurement result. Each plot shows the averaged value of three measurements and the error bar shows the 95% confidence interval. The reciprocal of P linearly increased with the fluid temperature T . The data in figure 10(a) are re-plotted in figure 10(b) in terms of the reciprocal of fluid viscosity μ . The viscosity of the measured temperature was obtained from the literature value for water [51] and the fitting curve based on Andrade equation [52]. In each measurement, $1/P$ shows linear relationship with $1/\mu$ and the gradient is same with that of the calibration line for sucrose solution in figure 6 which is also plotted in figure 10(b).

From equation (2), the direct effect of the change in T on P will appear as the change in the gradient. However, being inside the measurement uncertainty, the direct influence of T was not noticeable in figure 10(b). The direct effect was estimated to be 13% of the total influence calculated from equation (2) for the condition of temperature range of 22–40°C and using FITC water solution. Therefore, the relationship between the fluid temperature and polarization degree was mainly represented by the temperature dependence of the fluid viscosity in the present case. If the fluid has higher temperature dependence of viscosity compared to water, the direct influence of temperature is estimated to be even smaller. Hence, the viscosity change associated with temperature change can be measured using the calibration data obtained by varying the solute concentration under certain temperature, if the deviation associated with the direct influence of T on P is acceptable. It should be noted that if the concentration of the solution is constant and the temperature dependence of the solution viscosity is known, the calibration data obtained directly for the relationship between the polarization degree and temperature (as shown in figure 10(a)) will give a more accurate viscosity measurement.

5. Summary and conclusions

An optical measurement technique for in-situ and two-dimensional viscosity mapping in microscale was developed based on fluorescence polarization method. The optical system for polarization imaging was constructed using two synchronized cameras which simultaneously obtain the fluorescence images of different polarization components.

The proposed technique was applied to the measurement of viscosity distribution associated with concentration distribution under uniform and constant temperature condition. The relationship between the polarization degree P and fluid viscosity μ was experimentally evaluated at 30 °C using three kinds of fluorophores, and C-FITC was selected as viscosity probe in terms of reliability giving the largest P values among the three. The calibration experiment conducted in the range 0.7–3.0 mPa·s using C-FITC showed that the reciprocal of P showed a linear relationship with the reciprocal of fluid viscosity, which qualitatively agreed with the theoretical prediction. The calibration results obtained for sucrose and glucose solutions were almost equivalent, which supports the versatility of the present technique. The measurement uncertainty was estimated to be 7.5–9.5% corresponding to 0.07 mPa·s for 0 wt% sucrose solution (i.e., water) and 0.22 mPa·s for 35wt% sucrose solution. Viscosity measurement was performed in the Y-shaped microchannel to which two miscible solutions with different viscosities were supplied from each inlet. The viscosity distribution in the diffusion layer with the width of ~ 100 μm was successfully visualized in the flow direction at a spatial resolution of 1.3×1.3 μm^2 and agreed quantitatively with the result of numerical calculation. These results indicate the potential of the present technique for contributing to microscale analyses of chemical processes and biological fluids.

In addition to this, the polarization measurement was conducted for water at different temperature conditions (20–40 °C). The result showed a linear relationship between $1/\mu$ and $1/P$, which was comparable to the viscosity calibration result using sucrose solutions. The direct influence of temperature change on the polarization degree was estimated to be 13% of the total influence and the present technique could be applied to two-dimensional visualization of the viscosity distribution associated with temperature change with that accuracy.

Acknowledgments

This work was partially supported by JSPS Grant-in-Aid for Early-Career Scientists Grant Number JP18K13701 and JST COI Grant Number JPMJCE1307.

References

- 1 Manz A, Graber N and Widmer H M 1990 Miniaturized total chemical analysis systems: a novel concept for chemical sensing *Sensors Actuators B* **1** 244–8
- 5 2 Haeberle S and Zengerle R 2007 Microfluidic platforms for lab-on-a-chip applications *Lab Chip* **7** 1094–110
- 3 Patabadige D E W, Jia S, Sibbitts J, Sadeghi J and Sellens K and Culbertson C T 2016 Micro total analysis systems: fundamental advances and applications *Anal. Chem.* **88** 320–38
- 4 Wu C, Tang K, Gu B, Deng J, Liu Z and Wu Z 2016 Concentration-dependent viscous mixing in microfluidics: modelings and experiments *Microfluid. Nanofluid.* **20**(90) 11pp
- 10 5 Tice J D, Lyon A D and Ismagilov R F 2004 Effects of viscosity on droplet formation and mixing in microfluidic channels *Analytica Chimica Acta* **507** 73–7
- 6 Whorlow R W 1980 *Rheological techniques* Ellis Horwood, Chichester, UK.
- 7 Srivastava N, Davenport R D and Burns M A 2005 Nanoliter Viscometer for Analyzing Blood Plasma and Other Liquid Samples *Anal. Chem.* **77** 383–92
- 15 8 Pipe C J, Majmudar T S and McKinley G H 2008 High shear rate viscometry *Rheol. Acta* **47** 621–64
- 9 Bircher B A, Duempelmann L, Renggli K, Lang H P, Gerber C, Bruns N and Braun T 2013 Real-time viscosity and mass density sensors requiring microlitersample volume based on nanomechanical resonators *Anal. Chem.* **85** 8676–83
- 20 10 Guillot P, Panizza P, Salmon J-B, Joanicot M and Coli A 2006 Viscosimeter on a Microfluidic Chip *Langmuir* **22** 6438–45
- 11 Solomon D K and Vanapalli S A 2014 Multiplexed microfluidic viscometer for high-throughput complex fluid rheology *Microfluid. Nanofluid.* **16** 677–90
- 25 12 Li y, Ward K R, Burns M A 2017 Viscosity Measurements Using Microfluidic Droplet Length *Anal. Chem.* **89** 3996–4006
- 13 Kuimova M K 2012 Mapping viscosity in cells using molecular rotors *Phys. Chem. Chem. Phys.* **14** 12671–86
- 14 Lee S-C Heo J Woo H C Lee J-A Seo Y H Lee C-L Kim S and Kwon O-P 2018 Fluorescent Molecular Rotors for Viscosity Sensors *Chem. Eur. J.* **24** 13706–18
- 30 15 Kuimova M K, Yahioğlu G, Levitt J A and Suhling K 2008 Molecular Rotor Measures Viscosity of Live Cells via Fluorescence Lifetime Imaging *J. Am. Chem. Soc.* **130** (21) 6672–73
- 16 Mark A. Haidekkera and Emmanuel A 2007 Molecular rotors—fluorescent biosensors for viscosity and flow *Org. Biomol. Chem.* **5** 1669–78
- 35 17 Levitt J A Chung P-H Kuimova M K Yahioğlu G Wang Y Qu J and Suhling K 2011 Fluorescence Anisotropy of Molecular Rotors *Chem. Phys. Chem.* **12** 662–72
- 18 Kotani R Sotome H Okajima H Yokoyama S Nakaike Y Kashiwagi A Mori C Nakada Y Ymaguchi S Osuka A Sakamoto A Miyasaka H and Saito S 2017 Flapping viscosity probe that shows polarity-independent ratiometric fluorescence *J. Mater. Chem. C* **5** 5248–56

- 19 He F, Becker G W, Litowski J R, Narhi L O, Brems D N and Razinkov V I 2010 High-throughput dynamic light scattering method for measuring viscosity of concentrated protein solutions *Anal. Biochem.* **399** 141–3
- 20 Kim J and Ju T S 2008 Brownian Microscopy for Simultaneous In Situ Measurements of the
5 Viscosity and Velocity Fields in Steady Laminar Microchannel Flows *J. Microelectromech. Syst.* **17**(5) 1135–43
- 21 Swaminathan R, Hoang C P and Verkman A S 1997 Photobleaching recovery and anisotropy decay of green fluorescent protein GFP-S65T in solution and cells: cytoplasmic viscosity probed by green fluorescent protein translational and rotational diffusion *Biophys. J.* **72** 1900–7
- 10 22 Liang L, Wang X, Xing D and Chen T 2009 Noninvasive determination of cell nucleoplasmic viscosity by fluorescence correlation spectroscopy *J. Biomed. Opt.* **14**(2) 024013 9pp
- 23 Puchkov E O 2012 Single yeast cell vacuolar milieu viscosity assessment by fluorescence polarization microscopy with computer image analysis *Yeast* **29** 185–90
- 24 Dix J A and Verkman A S 1990 Mapping of fluorescence anisotropy in living cells by ratio
15 imaging Application to cytoplasmic viscosity *Biophys. J.* **57** 231–40
- 25 Benninger R K P, Hofmann O, McGinty J, Requejo-Isidro J, Munro I, Neil M A A, deMello A J and French P M W 2005 Time-resolved fluorescence imaging of solvent interactions in microfluidic devices *Opt. Exp.* **13**(16) 6275–85
- 26 Suhling K, Siegel J, Lanigan P M P, Lévêque-Fort S, Webb S E D, Phillips D, Davis D M and
20 French P M W 2004 Time-resolved fluorescence anisotropy imaging applied to live cells *Opt Lett.* **29**(6) 584–6
- 27 Jameson D M and Ross J A 2010 Fluorescence Polarization/Anisotropy in Diagnostics and Imaging *Chem. Rev.* **110** 2685–708
- 28 Smith D S and Eremin S A 2008 Fluorescence polarization immunoassays and related methods
25 for simple, high-throughput screening of small molecules *Anal. Bioanal. Chem.* **391** 1499–507
- 29 Yadavalli V K and Pishko M V 2004 Biosensing in microfluidic channels using fluorescence polarization *Analytica Chimica Acta* **507** 123–8
- 30 Tachi T, Kaji N, Tokeshi M and Baba Y 2009 Microchip-based homogeneous immunoassay using fluorescence polarization spectroscopy *Lab Chip* **9** 966–71
- 30 31 Choi J-W, Kang D-K, Park H, deMello A J and Chang S-I 2012 High-throughput analysis of protein–protein interactions in picoliter-volume droplets using fluorescence polarization *Anal. Chem.* **84** 3849–54
- 32 Tatsumi K, Hsu C-H, Suzuki A and Nakabe K 2018 Liquid temperature measurement method in microchannels by using fluorescence polarization *Heat Mass Trans.* **54** 2607–16
- 35 33 Suzuki A, Tatsumi K, Satoshi H, Kuriyama R and Nakabe K 2017 Temperature measurement in microchannel liquid flow by measuring fluorescence polarization *Trans. JSME (in Japanese)* **83**(853) 12pp
- 34 Perrin F 1929 La Fluorescence des Solutions. Induction Moléculaire – Polarisation et Durée D’émission – Photochimie *Ann. de Physique* **12** 169–275

- 35 Weber G 1953 Rotational Brownian motion and polarization of the fluorescence of solutions
Advances in Protein Chem., **8** 415–59
- 36 Walker D A 1987 A fluorescence technique for measurement of concentration in mixing fluids *J. Phys.* **20** 217–24
- 5 37 Feil H, Bae Y H, Feijen J and Kim S W 1991 Molecular separation by thermosensitive hydrogel Membranes *J. Membrane Sci.* **64** 283–94
- 38 Madge D, Rojas G E and Seybold P G 1999 Solvent dependence of the fluorescence lifetime of xanthene dyes *Photochem. Photobiol.* **70**(5) 737–44
- 39 Tsunomori F and Ushiki H 1999 Pore size effect on diffusion coefficient of rhodamine B in PNIPA gel *Phy. Lett. A* **258** 171–6
- 10 40 Dong C Y, So P T C, French T and Gratton E 1995 Fluorescence lifetime imaging by asynchronous pump-probe microscopy *Biophysical J.* **69** 2234–42
- 41 Cuenca A and Bodiguel H 2012 Fluorescence photobleaching to evaluate flow velocity and hydrodynamic dispersion in nanoslits *Lab Chip* **12** 1672–9
- 15 42 Kawski A 1983 Excitation energy transfer and its manifestation in isotropic media *Photochem. Photobiol.* **38** 487–508
- 43 Jablónski A 1960 On the notion of emission anisotropy, Bulletin of the Polish Academy of Sciences Series A, **8** 259–64
- 44 Dreier T, Blaser S, Kinzelbach W, Virant M and Maas H-G 2000 Simultaneous measurement of particle and fluid velocities in a plane mixing layer with dispersion *Exp. Fluids* **29** 486–93
- 20 45 Russ J C 2007 *The Image Processing Handbook 5th edn* (Boca Raton: CRC/Taylor and Francis)
- 46 Soloff S M, Adrian R J and Liu Z-C 1997 Distortion compensation for generalized stereoscopic particle image velocimetry *Meas. Sci. Technol.* **8** 1441–54
- 47 Laurent T C and Öbrink B 1972 On the restriction of the rotational diffusion of proteins in polymer networks *Eur. J. Biochem.* **28**, 94–101.
- 25 48 Contreras-Lopez E, Champion D, Hervet H, Blond G and Le Meste M 2000 Rotational and translational mobility of small molecules in sucrose plus polysaccharide solutions *J. Agric. Food Chem.* **48** 1009–15
- 49 Bates F J and associates 1942 Polarimetry, saccharimetry and the sugars Circular C440 of the National Bureau of Standards (Washington, D.C.: United States Government Printing Office)
- 30 50 Henrion P N Diffusion in the sucrose+ water system 1964 *Trans. Faraday Soc.* **60** 72–4
- 51 Japan Society of Thermophysical Properties 2000 *Thermophysical Properties Handbook 2nd edn* (Tokyo: Yokendo Ltd)
- 52 Andrade E N C 1930 The viscosity of liquids, *Nature* **125** (3148) 309–10
- 35

List of tables

Table 1	Optical components for fluorescence measurement
Table 2	Properties of the fluorophores applied to equation (2) to estimate the viscosity dependence of polarization degree

List of figures

Figure 1	Schematic of the polarization characteristics of the fluorescence in the cases of (a) fluorophores in stationary state and (b) those dissolved in solution. Upper figures show the relationship between the linearly-polarized excitation light and fluorescence polarization. Lower figures show the probability density distributions of the angle between the excitation polarization direction (along z-axis) and absorption/emission dipole moments (shown in black and gray dotted line, respectively).
Figure 2	Schematic of the optical system for polarization measurement using an inverted microscope.
Figure 3	Top and cross-sectional views of (a) straight microchannel used for calibration experiment and (b) Y-shaped microchannel used for viscosity distribution measurement. (c) The measurement area located downstream of the junction. (d) Computational domain for the three-dimensional numerical simulation of mass transport in microchannel flow. The height and width are same as the Y-shape microchannel.
Figure 4	(a) Example of P distribution obtained from 35wt% sucrose solution before subtracting the systematic error and (b) the resultant distribution after the error correction procedure.
Figure 5	Relationship between the reciprocal of the fluid viscosity $1/\mu$ and polarization degree P in the case of C-FITC, rhodamine B and uranine. The solid lines represent the theoretical values obtained by applying the values shown in table 2 to equation (2).
Figure 6	Relationship between the reciprocal of the fluid viscosity $1/\mu$ and the reciprocal of the polarization degree $1/P$ in the cases of sucrose and glucose solutions. The straight lines were obtained based on the least square approximation.
Figure 7	Comparison of variations in fluorescence intensity I and polarization degree P measured on different day. I and P are normalized by the values of Day 1.
Figure 8	(a) Viscosity distribution in the Y-shaped microchannel obtained by polarization measurement. Distribution of polarization degree P was converted to the fluid viscosity μ using the calibration line for sucrose solution shown in figure 6. (b) Viscosity distribution obtained by numerical computation. The

distribution of sucrose concentration was calculated in the domain shown in figure 3(d) and converted to the fluid viscosity μ .

Figure 9 Comparison of spanwise distributions of fluid viscosity at $x=10 \mu\text{m}$ and $900 \mu\text{m}$ obtained by polarization measurement and numerical calculation.

5 Figure 10 (a) Relationship between the fluid temperature T and the reciprocal of the polarization degree ($1/P$) obtained using C-FITC in water. (b) The values in figure 10(a) are plotted again in terms of the reciprocal of water viscosity $1/\mu$ and compared with the viscosity calibration data in figure 6.

10

Table 1. Optical components for fluorescence measurement

	C-FITC and uranine	Rhodamine B
LED light	Thorlabs; M490L4	Thorlabs; M565L3
Excitation filter	Semrock; FF01-482/35	Semrock; FF01-536/35
Dichroic mirror	Semrock; FF506-Di03	Olympus; DM570
Emission filter	Semrock; FF01-536/40	Olympus; BA575IF

5 **Table 2.** Properties of the fluorophores applied to equation (2) to estimate the viscosity dependence of polarization degree

	Uranine	Rhodamine B	C-FITC	FITC
Molecular weight	376.27	479.01	26000	389.38
Diameter [nm]	1.03 ^[37]	1.6 ^[39]	30 ^[32]	1.28 ^[41]
Fluorescence lifetime [ns]	4.16 ^[38]	1.44 ^[40]	4.16 ^[38]	4.16 ^[38]
Excitation wavelength [nm]	490	555	494	494
Emission wavelength [nm]	520	580	520	520

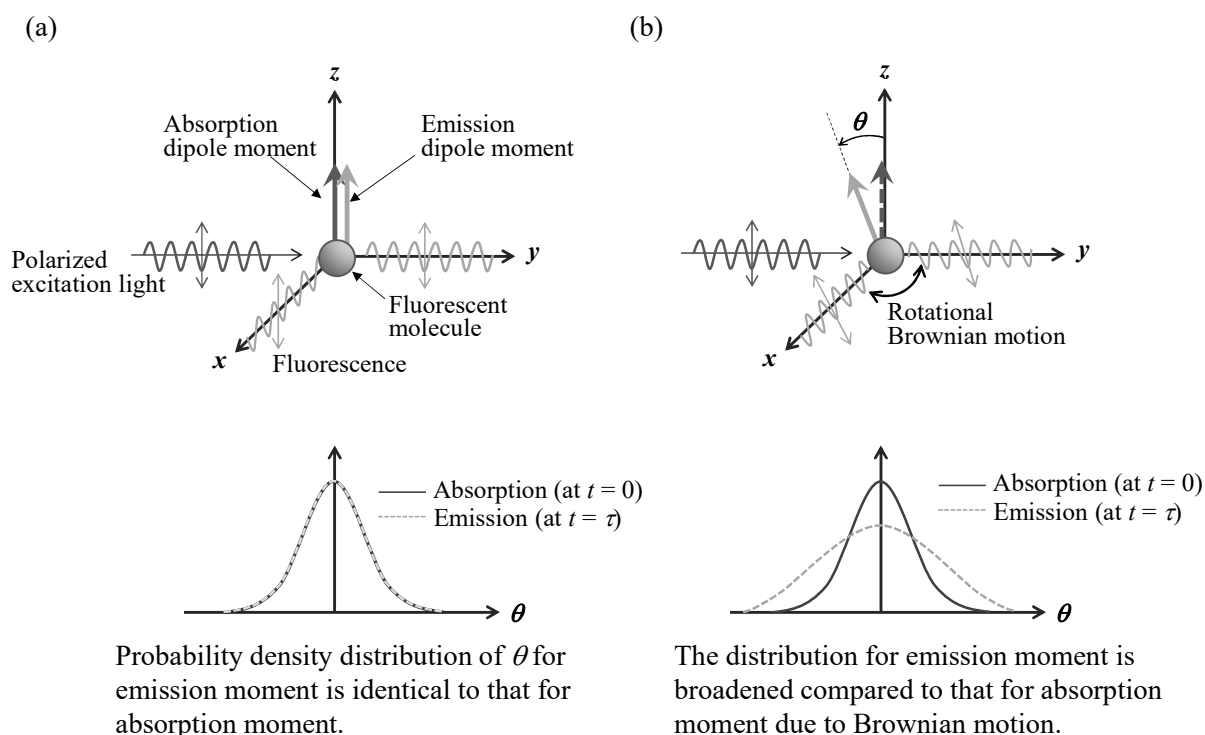
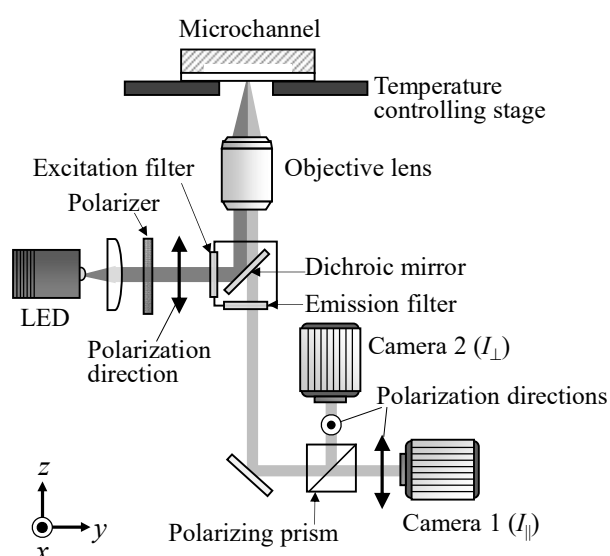
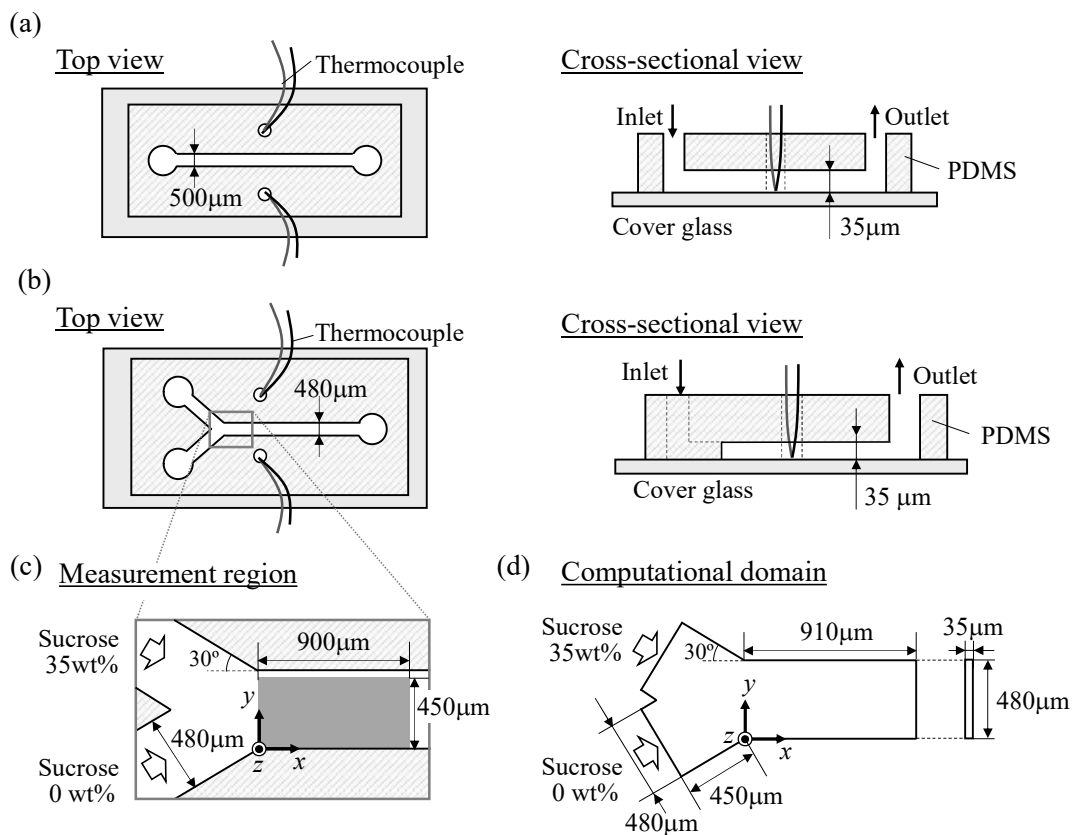


Figure 1. Schematic of the polarization characteristics of the fluorescence in the cases of (a) fluorophores in stationary state and (b) those dissolved in solution. Upper figures show the relationship between the linearly-polarized excitation light and fluorescence polarization. Lower figures show the probability density distributions of the angle between the excitation polarization direction (along z -axis) and absorption/emission dipole moments (shown in black and gray dotted line, respectively).



10

Figure 2. Schematic of the optical system for polarization measurement using an inverted microscope.



5 **Figure 3.** Top and cross-sectional views of (a) straight microchannel used for calibration experiment and (b) Y-shaped microchannel used for viscosity distribution measurement. (c) The measurement area located downstream of the junction. (d) Computational domain for the three-dimensional numerical simulation of mass transport in microchannel flow. The height and width are same as the Y-shape microchannel.

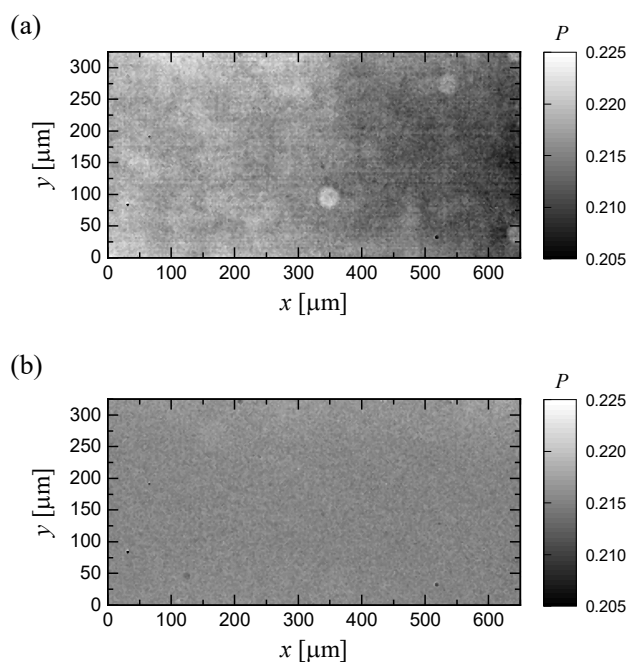


Figure 4. (a) Example of P distribution obtained from 35wt% sucrose solution before subtracting the systematic error and (b) the resultant distribution after the error correction procedure.

5

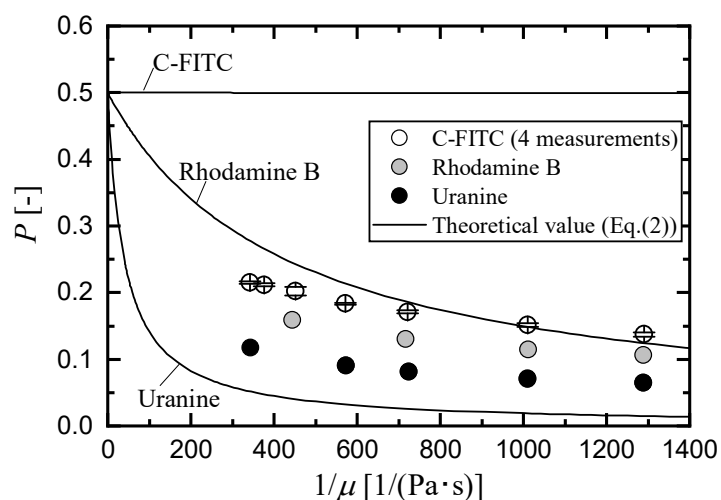
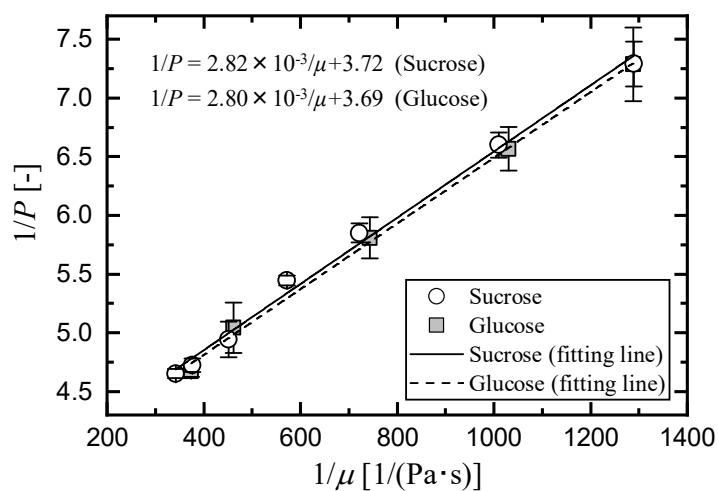
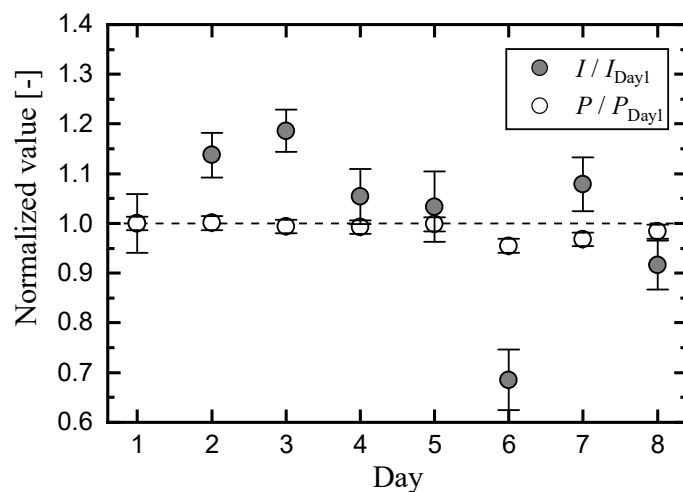


Figure 5. Relationship between the reciprocal of the fluid viscosity $1/\mu$ and polarization degree P in the case of C-FITC, rhodamine B and uranine. The solid lines represent the theoretical values obtained by applying the values shown in table 2 to equation (2).

10



5 **Figure 6.** Relationship between the reciprocal of the fluid viscosity $1/\mu$ and the reciprocal of the polarization degree $1/P$ in the cases of sucrose and glucose solutions. The straight lines were obtained based on the least square approximation.



10 **Figure 7.** Comparison of variations in fluorescence intensity I and polarization degree P measured on different day. I and P are normalized by the values of Day 1.

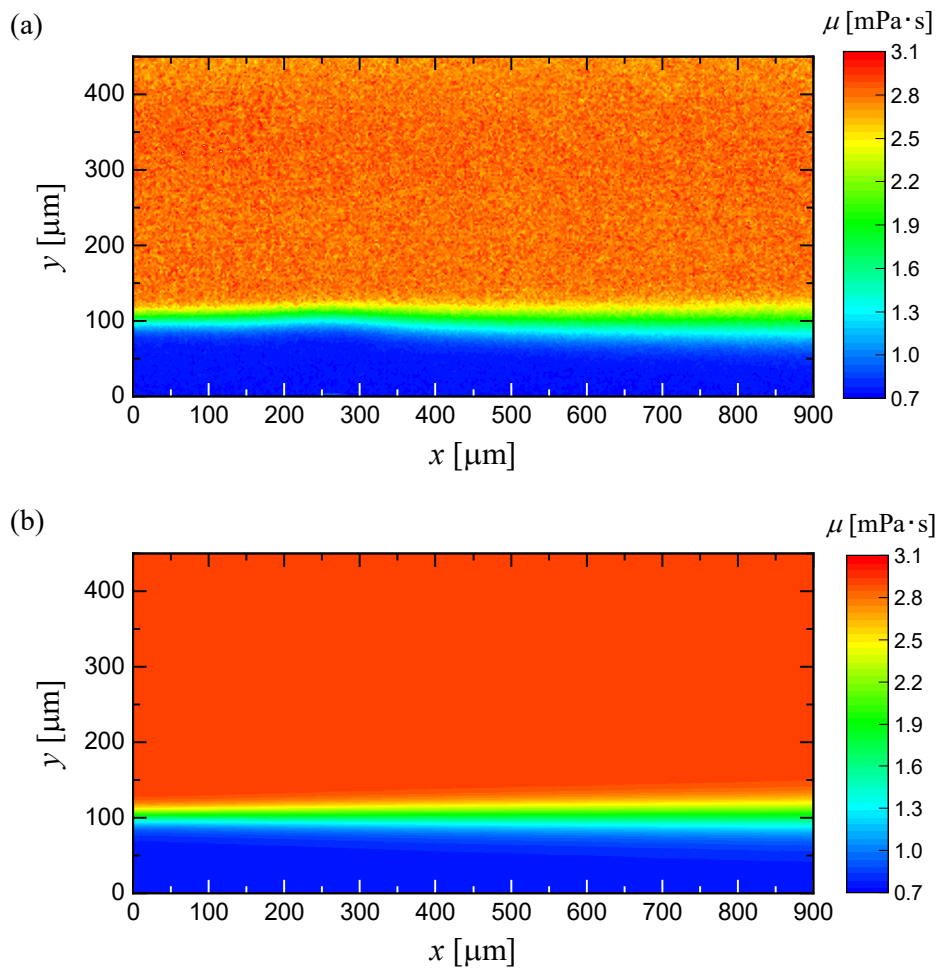


Figure 8. (a) Viscosity distribution in the Y-shaped microchannel obtained by polarization measurement. Distribution of polarization degree P was converted to the fluid viscosity μ using the calibration line for sucrose solution shown in figure 6. (b) Viscosity distribution obtained by numerical computation. The distribution of sucrose concentration was calculated in the domain shown in figure 3(d) and converted to the fluid viscosity μ .

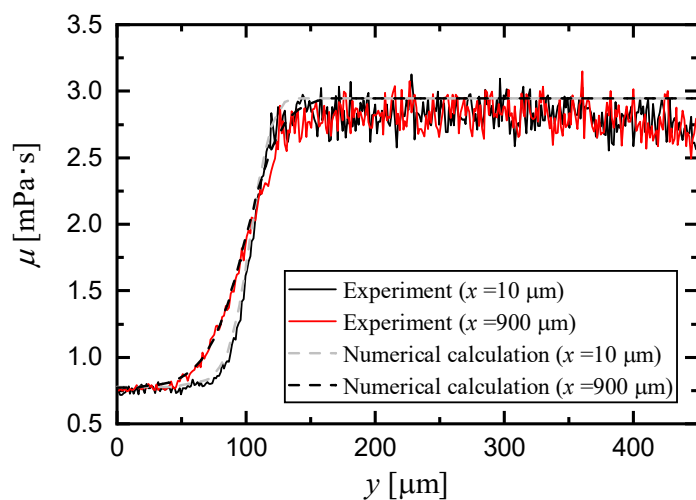
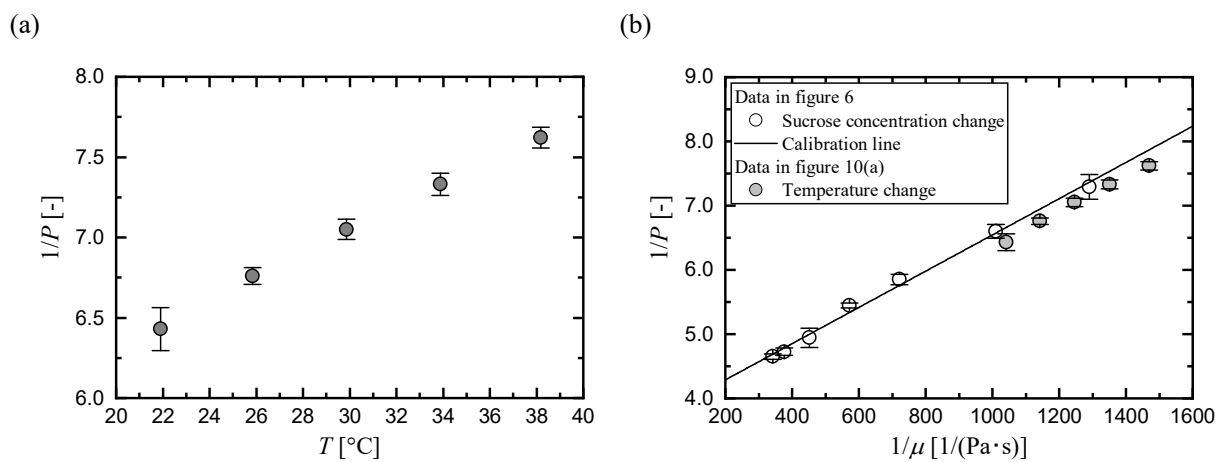


Figure 9. Comparison of spanwise distributions of fluid viscosity at $x=10 \mu\text{m}$ and $900 \mu\text{m}$ obtained by polarization measurement and numerical calculation.

5



10

Figure 10. (a) Relationship between the fluid temperature T and the reciprocal of the polarization degree ($1/P$) obtained using C-FITC in water. (b) The values in figure 10(a) are plotted again in terms of the reciprocal of water viscosity $1/\mu$ and compared with the viscosity calibration data in figure 6.

Supplementary Material for:

Two-dimensional fluid viscosity measurement in microchannel flow using fluorescence polarization imaging

Reiko KURIYAMA*, Tomotaka NAKAGAWA, Kazuya TATSUMI, Kazuyoshi NAKABE

Department of Mechanical Engineering and Science, Graduate School of Engineering, Kyoto University

Kyoto daigaku-katsura, Nishikyo-ku, Kyoto 615-8540, JAPAN

* To whom correspondence should be addressed.

Tel: +81-75-383-3608

Fax: +81-75-383-3608

E-mail: kuriyama.reiko.2m@kyoto-u.ac.jp

This Supplementary Information includes the descriptions for the research article entitled “Two-dimensional fluid viscosity measurement in microchannel flow using fluorescence polarization imaging.” Details for the evaluation of the concentration depolarization of fluorophores, and the viscosity dependence of the polarization degree are provided.

Evaluation of concentration depolarization

To obtain sufficient fluorescence intensity and polarization signal, the concentration of fluorophore should be determined carefully considering the effect called concentration depolarization. When the concentration of fluorophores is higher than a certain value, i.e., the separation distance between fluorophores is sufficiently small (up to ~ 10 nm), radiationless excitation energy transfer occurs from primarily excited molecules (donors) to the surrounding unexcited molecules (acceptors). In this case, the acceptors emit depolarized fluorescence and the polarization degree of the measured fluorescence is decreased as a whole. This phenomenon is called concentration depolarization, alternatively self-depolarization or polarization quenching [S1], and its degree is highly dependent on the separation between donor and acceptor, i.e., the concentration of fluorophores. Here, the influence of the concentration depolarization is estimated based on the theoretical equation proposed by Jablónski [S2], which is expressed as,

$$\frac{r}{r_0} = \frac{2(\nu - 1 + e^{-\nu})}{\nu^2}, \quad (\text{S1})$$

where r is fluorescence anisotropy defined as $r \equiv (I_{\parallel} - I_{\perp}) / (I_{\parallel} + 2I_{\perp}) = 2P / (3 - P)$, and r_0 is the maximum fluorescence anisotropy observed when no depolarization effects are present. ν represents the average number of fluorophores (acceptors) within a so-called “active sphere”, expressed as,

$$\nu = \frac{4}{3} \pi R_s^3 \left[1 - \langle \kappa^2 \rangle \left(\frac{R_0}{R_s} \right)^6 \right] n_d, \quad (\text{S2})$$

where R_s [nm] is the effective range of the Förster interaction and corresponds to the radius of the active sphere. R_0 [nm] is the Förster separation distance at which the energy transfer efficiency is 50%, n_d [m⁻³] is the number density of the fluorophore, and $\langle \kappa^2 \rangle$ is a factor depending on the mutual orientation of the transition moments of the interacting molecules [S1]. Figure S1(a) shows the relationships between the fluorophore concentration C [mol l⁻¹] and r/r_0 calculated for the three fluorophores. For fluorescein and rhodamine B, the properties listed in table S1 were applied to equation (S2). Note that uranine and FITC are both derivatives of fluorescein and therefore their fluorescence behaviors are expected to be quite similar to one another. In figure S1(a), r/r_0 decreases notably in the range $C = 10^{-4}$ – 10^{-2} mol/l and falls to almost 0 at $C = 10^{-1}$ mol/l for both fluorescein and rhodamine B. This means that the accuracy of polarization measurement decreases when $C > 10^{-4}$ mol/l. The theoretical curve of rhodamine B was compared with experimental values and a good agreement was confirmed in our previous report [S3].

In the case of C-FITC, the degree of concentration depolarization should be evaluated with taking into account its molecular structure. C-FITC is a casein molecule whose surface is labeled with several FITCs. Since the molecular weight (Mw) of FITC is ~ 389 , the number of FITCs linked to a single casein molecule, m_{FITC} , is estimated to be ~ 20 from the difference in molecular weight between κ -casein (Mw ~ 19000) and C-FITC (Mw ~ 26000). The densely distributed FITCs are expected to cause concentration depolarization within a single C-FITC. Moreover, the size of the active sphere of C-FITC is supposed to be different from that of a simple FITC molecule. To take this into the consideration, ν was calculated as follows assuming that the active sphere of C-FITC is represented by a simple model shown in figure S1(b),

$$\nu = \int_d^{d+R_s} n_d \times m_{\text{FITC}} \times 4\pi r^2 dr, \quad (\text{S3})$$

where d is the diameter of C-FITC. The degree of concentration depolarization can then be estimated by equation (S1) but it should be noted that r_0 of the case of C-FITC represents the anisotropy when only the concentration depolarization between FITCs on the same C-FITC molecule takes place and that between neighboring C-FITC molecules is negligible. Black solid line in figure S1(a) shows the concentration dependence of r/r_0 for C-FITC. The concentration depolarization occurs at $C > 10^{-7}$ mol/l and the fluorescence is almost completely depolarized at $C = 10^{-4}$ mol/l. This result indicates that C should be lower than 10^{-6} mol/l to avoid significant influence of concentration depolarization. On the other hand, such low concentration leads to the difficulty in the measurement of extremely weak fluorescence. In addition to this, the sensitivity of the polarization degree P on fluorophore

concentration is high at $C < 10^{-5}$ mol/L as shown in figure S1(c), which leads to the considerable change in P when the fluorophore concentration fluctuates. When the C-FITC concentration is controlled around 4.0×10^{-5} mol/l, the influence of the concentration variation within $\pm 5\%$ on measured viscosity value is estimated to be about $\pm 1.6\%$ in the present viscosity range.

To obtain sufficient intensity while suppressing the influence of concentration depolarization, the fluorophore concentration was set to be 4.0×10^{-5} mol/l for C-FITC and 1.0×10^{-4} mol/l for uranine and rhodamine B in the present study.

Table S1. Properties of the fluorophores applied to equation (S2) to estimate the degree of concentration depolarization (from Ref [S1]).

	Fluorescein	Rhodamine B
R_0 [nm]	4.18	5.03
R_s/R_0	1.6	1.6
$\langle \kappa^2 \rangle$	0.476	0.476

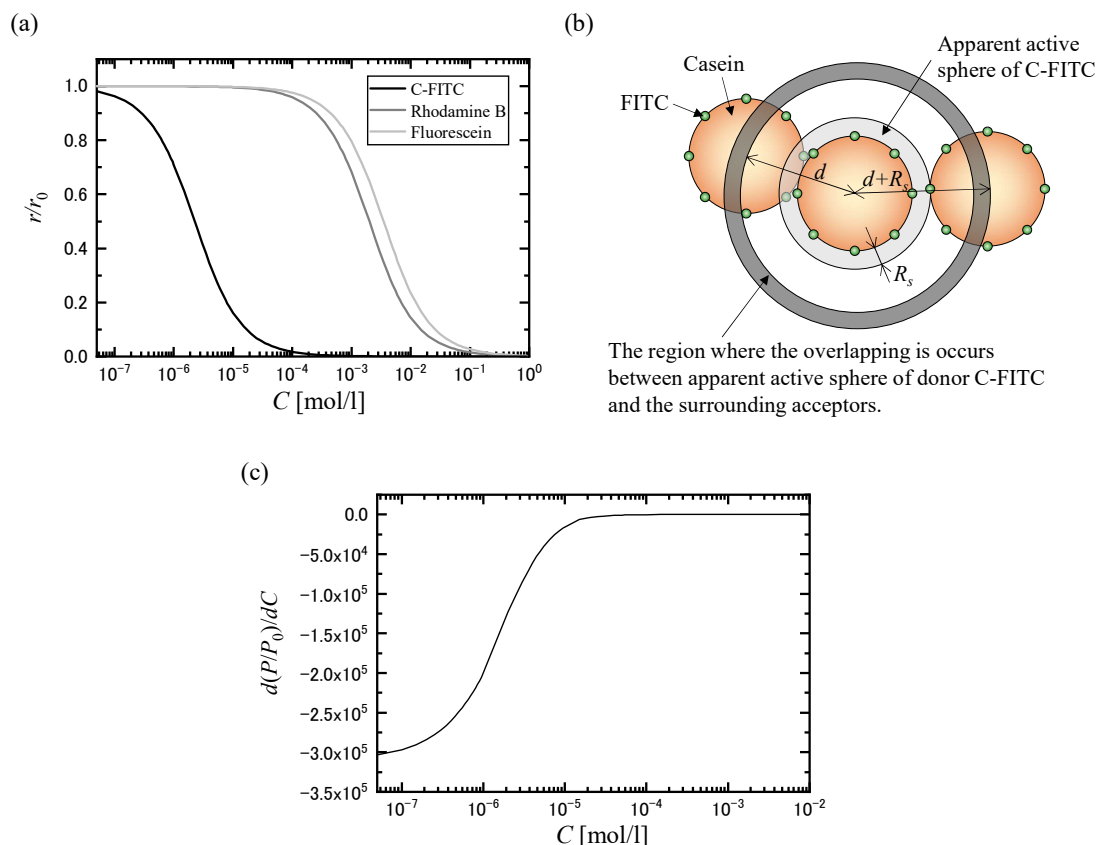


Figure S1. (a) Relationship between the fluorophore concentration C and the degree of concentration depolarization r/r_0 calculated for C-FITC, rhodamine B, and fluorescein. (b) Schematic of the model for the apparent active sphere of C-FITC and the region where the donor-acceptor energy transfer occurs. (c) The sensitivity $d(P/P_0)/dC$ plotted against the concentration.

Viscosity dependence of the depolarization degree

The theoretical equation which relates P value to the fluorescence lifetime and the rotational diffusion of fluorophores is expressed as follows:

$$\left(\frac{1}{P} - \frac{1}{3}\right) = \left(\frac{1}{P_0} - \frac{1}{3}\right) \left(1 + \frac{k_B T \tau}{\mu V}\right), \quad (\text{S4})$$

where k_B [J/K] is the Boltzmann constant, V [m³] is the hydrodynamic volume of the rotating unit, and τ [s] is the fluorescence lifetime. T [K] and μ [Pa·s] are the absolute temperature and viscosity of the fluid, respectively. P_0 is the intrinsic or limiting polarization defined as the polarization degree of the molecule at stationary condition (in the absence of rotation). From this equation, we obtain the following relationship:

$$P = \frac{\mu P_0}{\mu + \left(1 - \frac{P_0}{3}\right) \frac{k_B T \tau}{V}}, \quad (\text{S5})$$

and the viscosity dependence of P value:

$$\frac{\partial P}{\partial \mu} = \frac{P_0 \left(1 - \frac{P_0}{3}\right) \frac{k_B T \tau}{V}}{\left[\mu + \left(1 - \frac{P_0}{3}\right) \frac{k_B T \tau}{V}\right]^2}. \quad (\text{S6})$$

From equation (S6), it is clear that the viscosity dependency of P becomes lower and when μ increases. This results in the larger deviation in the 35wt% sucrose solution area in figure 9 as explained in the last paragraph of subsection 4.2.

References for Supplementary Material

- (S1) Kawski A 1983 Excitation energy transfer and its manifestation in isotropic media *Photochem. Photobiol.* **38** 487–508
- (S2) Jablónski A 1960 On the notion of emission anisotropy, *Bulletin of the Polish Academy of Sciences Series A* **8** 259–64
- (S3) Suzuki A, Tatsumi K, Satoshi H, Kuriyama R and Nakabe K 2017 Temperature measurement in microchannel liquid flow by measuring fluorescence polarization Trans. JSME (in Japanese) **83**(853) 12pp